Spatiotemporal seismicity pattern of the Taiwan orogen

Yi-Ying Wen[1, 2*], Chien-Chih Chen[3, 4], Strong Wen[1, 2], and Wei-Tsen Lu[1]

[1]Department of Earth and Environmental Sciences, National Chung Cheng University, Chia-yi County 62102, Taiwan

[2]Environment and Disaster Monitoring Center, National Chung Cheng University, Chia-yi County 62102, Taiwan

[3]Department of Earth Sciences, National Central University, Taoyuan City 32001, Taiwan

[4]Earthquake-Disaster & Risk Evaluation and Management Center, National Central University, Taoyuan City 32001, Taiwan

Correspondence: Yi-Ying Wen (yiyingwen@ccu.edu.tw)

Abstract

We investigate the temporal and spatial seismicity patterns prior to eight M>6 events nucleating in different regions of Taiwan through a region-time-length algorithm and an analysis of a self-organizing spinodal model. Our results show that the spatiotemporal seismicity variations during the preparation process of impending earthquakes display distinctive patterns corresponding to tectonic settings. Q-type events occur in southern Taiwan and experience a seismic quiescence stage prior to the mainshock. A seismicity decrease of 2.5<M<4.5 events occurs around the relatively high b-value southern Central Range, which contributes to the accumulation of tectonic stress for preparing for the occurrence of the Q-type event. On the other hand, A-type events occur in central Taiwan and experience a seismic activation stage prior to the mainshock, which nucleates on the edge of the seismic activation area. We should pay attention when accelerating seismicity of 3<M<5 events appears within the low b-value area, which could promote the nucleation process of the A-type event.

1. Introduction

Seismic activity is related to spatiotemporal variations in the stress field and state, and seismicity changes prior to a large earthquake have been widely observed through different techniques, e.g., b-value analysis (Chan et al., 2012; Wyss and Stefansson, 2006), noncritical precursory accelerating seismicity theory (PAST) (Mignan and Giovambattista, 2008), pattern informatics (PI) algorithm (Rundle et al., 2003; Chen et al., 2005), the region-time-length (RTL) algorithm (Chen and Wu, 2006; Wen et al., 2016), and the analysis of self-organizing spinodal (SOS) model (Rundle et al., 2000). Previous studies have mostly focused on a significant earthquake; therefore, it is not easy to understand whether the properties of seismic activation and quiescence patterns respond to regional tectonic stress.

The Taiwan orogenic belt, which is an active and ongoing arc–continent collision zone as a result of the Philippine Sea Plate (PSP) obliquely colliding with the Eurasian Plate (EP), is particularly complex due to the two adjacent subduction zones, the Ryukyu trench and Manila trench to the northeast and south of the island, respectively (Suppe, 1984; Yu et al., 1997). The frequent and significant seismic activities as well as a rapid convergence rate of 85 to 90 mm/yr are well observed by the island-wide GPS and seismic networks (Fig. 1). The growth of the Taiwan orogenic belt shows propagation from north to south due to oblique plate convergence and opposing subduction in the southern and northern parts of Taiwan (Suppe, 1984). The central part of Taiwan, which is experiencing rapid to full collision, mainly consists of the Coastal Range, Central Range and Western Foothills (Shyu et al., 2005a; b). A myriad of active and thin-skinned structures are the products of the accretion of the continental sliver to the continental margin. In southern Taiwan, the EP subducting eastward beneath the PSP is in a stage of incipient arc–continent collision (Kao et al., 2000; Shyu et al., 2005a; b). The

55 northwest domain of southern Taiwan, which represent the southern tip of the fold-and-

56 thrust belt in the coastal plain and foothill region and show very low seismicity, mainly

57 consist of Miocene shallow marine deposits and a Pliocene–Pleistocene foreland basin

58 as well as mudstones.
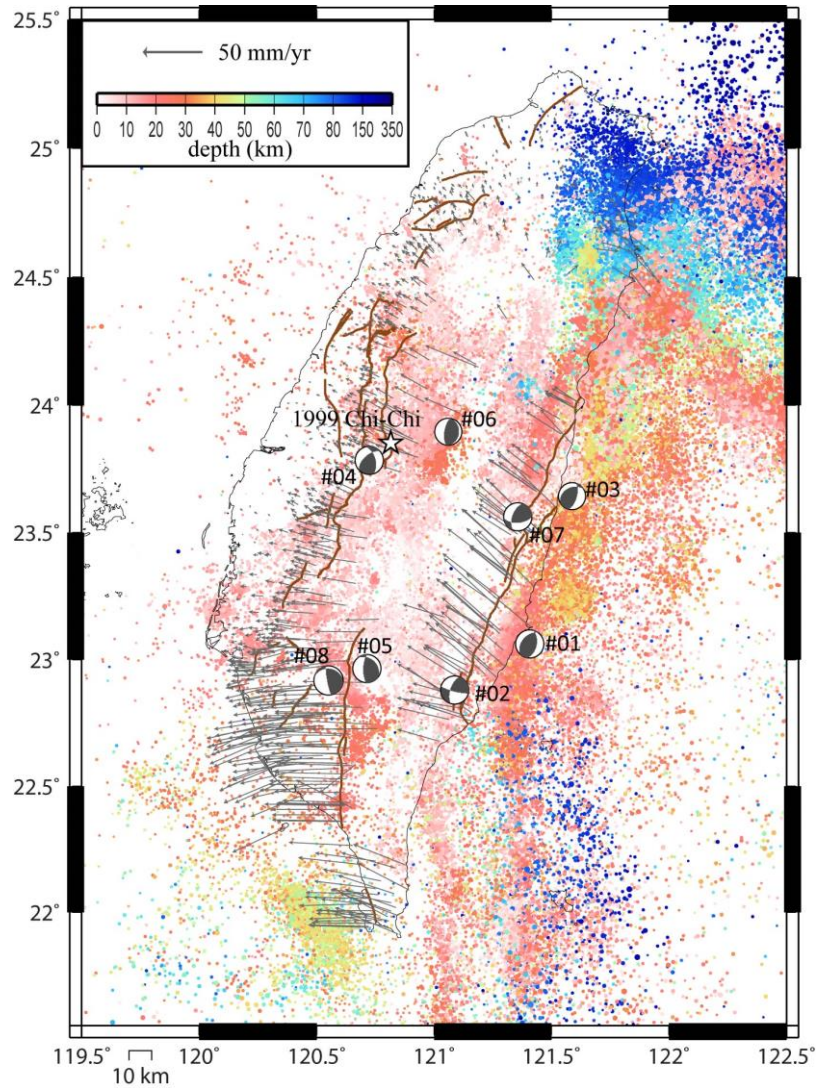
Figure 1: Horizontal velocities from 2002 to 2017 (Chen et al., 2018) and seismicity between 1991 and 2018. The white star shows the location of the 1999 Chi-Chi earthquake, and the focal mechanisms determined by the Global CMT soultion represent the locations of the investigated events in this study. The active faults (thick lines) identified by the Central Geological Survey of Taiwan are also shown.

59

60 Over the last two decades, several moderate earthquakes have occurred with various

61 seismicity patterns and in GPS velocity field regions. We investigate the temporal and

62 spatial seismicity patterns prior to eight M>6 events nucleated in different regions of

63 Taiwan through the RTL algorithm and analysis of the SOS model. Our attempt is not

64 to catch the seismic precursor but to focus on the seismicity changes related to the

65 regional tectonics, which might become useful hints for potential seismic hazard

66 assessments. The results show that the temporal and spatial seismicity (2.5<M<5)

67 variations during the preparation process of impending earthquakes could display

68 distinctive patterns corresponding to the tectonic setting.

69

70 **2. RTL Algorithm and Data**

71 The region-time-length (RTL) algorithm (Sobolev and Tyupkin, 1997; 1999) is a

72 statistical technique to detect the occurrence of seismic quiescence and activation by

73 taking into account the location, occurrence time and magnitude of earthquakes. The

74 RTL value is defined as the product of the three dimensionless factors, R, T and L:

75
$$R(x,y,z,t) = \left[\sum_{i=1}^{n} \exp\left(-\frac{r_i}{r_0}\right) \right] - R_{bk}(x,y,z,t) \tag{1}$$

76
$$T(x,y,z,t) = \left[\sum_{i=1}^{n} \exp(-\frac{t-t_i}{t_0}) \right] - T_{bk}(x,y,z,t) \tag{2}$$

77
$$L(x,y,z,t) = \left[\sum_{i=1}^{n} (\frac{l_i}{r_i}) \right] - L_{bk}(x,y,z,t) \tag{3}$$

78 where r_i is the distance between the investigated point (x, y, z) and the ith prior event

79 (with the occurrence time t_i and rupture length l_i). n is the number of prior events that

80 occurred in a defined space–time window with $r_i \leq 2r_0$ (r_0, characteristic distance) and

81 $(t - t_i) \leq 2t_0$ (t_0 , characteristic time-span). Rupture length l_i is a function of

82 earthquake magnitude (M_i), $\log l_i = 0.5M_i - 1.8$ (Kasahara, 1981). The weighted RTL

83 value reflects the deviation from the background seismicity level (R_{bk}, T_{bk} and L_{bk}) with

84 negative values for seismic quiescence and positive values for activation. r_0

85 characterizes the decreasing influence of more distant events, and t_0 describes the

86   reducing influence rate of the preceding events as the time of calculation moving on. To

87   diminish the ambiguity in determining the characteristic parameters, we follow the

88   systematic procedure of correlation analysis over pairs of RTL results proposed by

89   Huang and Ding (2012) to obtain the optimal model parameters, $\tilde{r_0}$ and $\tilde{t_0}$, of each

90   event. Details of this technique of correlation analysis are described in Appendix A. We

91   calculate various combinations of r_0 (ranging between 25 and 80 km with a step of 2.5

92   km) and t_0 (ranging between 0.25 and 2.0 yr with a step of 0.05 yr). As the correlation

93   coefficient criterion C_0 is set, we can calculate the ratio W (or weight) of the combination

94   with correlation coefficients equal to or larger than C_0 for each model parameter of r_{0i}

95   ($i=1 \sim m$; $m=23$) and t_{0j} ($j=1 \sim n$; $n=36$).

96   After testing many criterion sets, the criterion coefficient $C_0 = 0.6$ and criterion ratio

97    $W_0 = 0.5$ are acceptable for each event, which represents at least 50% of the total

98   combination pairs with correlation coefficient $C \geq C_0 = 0.6$. Then, we obtain the average

99    $\tilde{r_0} = 49.6$ km and average $\tilde{t_0} = 1.16$ yr. These model parameters are similar to those of

100   previous studies for Taiwan (Chen and Wu, 2006; Wen et al., 2016; Lu, 2017; Wen and

101   Chen, 2017).

102   For statistical analyses, catalog completeness is an important factor. Since 1991,

103   the Taiwan Telemetered Seismographic Network (TTSN) (Wang, 1989) has merged

104   with the Central Weather Bureau (CWB) seismic network and updated to an integrated

105   earthquake observation system, named the Central Weather Bureau Seismic Network

106   (CWBSN). Wang et al. (1994) pointed out that most shallow earthquakes occurring in

107   Taiwan are distributed at depths less than 35 km. According to previous studies (Wu

108   and Chiao, 2006; Wu et al., 2008; Wen et al., 2016; Hsu et al., 2021), we used the

109   earthquake catalog maintained by the CWB for the entire Taiwan area with M≥2.5 and

110   depth≤35 km between 1991 and 2018 and applied a declustering procedure proposed by

111 Gardner and Knopoff (1974). Considering a sufficient background seismicity and

112 minimizing the influence of the 1999 Chi-Chi earthquake, we only selected the M>6

113 inland earthquakes between 2003 and 2016 in Taiwan. Since two events occurring in a

114 close space–time window would show high similarity in RTL function (Lu, 2017), we

115 excluded the event occurring within $2\tilde{t}_0$ and $\tilde{r}_0$ with respect to the last M>6 events. For

116 example, two M>6 events within a distance of 10 km struck the Nantou area on 27

117 March 2013 and 02 June 2013, and we only analyzed the former event. Therefore, we

118 have eight qualified M>6 events, as listed in Table 1.

119

120 **Table 1**: Earthquake parameters for the investigated events determined by the CWB.

No.	Date (UT)	Long. (deg.)	Lat. (deg.)	Depth (km)	M_L
1	2003/12/10 04:38:14	121.398	23.067	17.7	6.4
2	2006/04/01 10:02:20	121.081	22.884	7.2	6.2
3	2009/10/03 17:36:06	121.579	23.648	29.2	6.1
4	2009/11/05 09:32:58	120.719	23.789	24.1	6.2
5	2010/03/04 00:18:52	120.707	22.969	22.6	6.4
6	2013/03/27 02:03:20	121.053	23.902	19.4	6.1
7	2013/10/31 12:02:10	121.349	23.566	15.0	6.4
8	2016/02/05 19:57:26	120.544	22.922	14.6	6.6

121

122 **3. Results**

123 **3.1 Temporal seismicity variation**

124 The temporal variation in the RTL function represents the different stages of

125 seismicity rate change at the target location with respect to the background level. For

126 consistency, we adopt a 10-year catalog as the background for each investigated event.

127 Figure 2 shows the temporal variation in the RTL functions prior to the investigated

events. We can see that before the occurrence of the investigated event, both seismicity

changes are observed: the seismic quiescence stage for Nos. 1, 2, 5 and 8 (Q-type events

hereafter) and the seismic activation stage for Nos. 3, 4, 6 and 7 (A-type events hereafter).

Q-type events occurred at different locations in southern Taiwan, and most, 3 among 4,

of their temporal RTL functions exhibit the seismic quiescence stages during 2002–

2004, which was before the occurrence of the 2003 Chengkung earthquake, i.e., event

No. 1. The seismicity increase (activation stage) took approximately two years following

the 2003 Chengkung mainshock (event No. 1). We note that the length of the seismic

quiescence stage prior to the Q-type event might correspond to the magnitude.
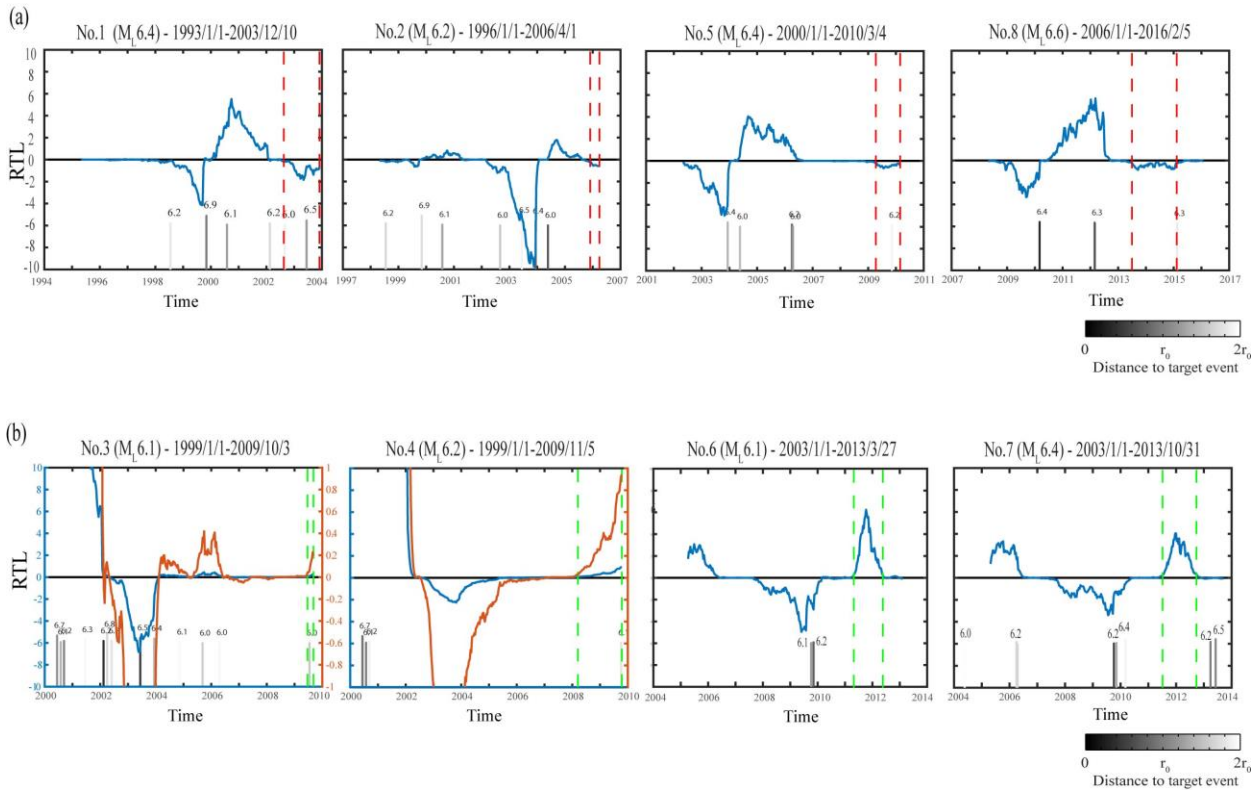
Figure 2: Temporal variation of the RTL function (blue line) for (a) Q-type events and (b) A-type events. The orange curves and vertical axes on the right represent the enlarged RTL functions of event Nos. 3 and 4. The vertical dashed red lines mark the seismic quiescence stage, and the vertical dashed green lines mark the seismic activation stage. The bar chart represents the occurrence time of $M \geq 6.0$ events within a distance of $2r_0$ from the target event; each number above the bar is the magnitude.

138 A-type events all occurred in central Taiwan and were located within $2\tilde{r}_0$ with

139 respect to the 1999 Chi-Chi earthquake. Figure 3 shows the declustered seismicity

140 distribution as a function of time and latitude. Significant seismicity followed the 1999

141 Chi-Chi earthquake north of 23°N. Since the background seismicity of event Nos. 3 and

142 4 started from 1999/01/01, the RTL functions were obviously affected by the occurrence

143 of the 1999 Chi-Chi earthquake. Therefore, we enlarge the vertical axis to accentuate

144 the seismicity variation prior to event Nos. 3 and 4. As shown in Fig. 2, the temporal

145 RTL functions of A-type events mostly show a seismic activation stage between 2004

146 and 2006, which corresponds to the seismicity increase following the 2003 Chengkung

147 mainshock (event No. 1). However, for the A-type event, we could not see the

148 relationship between the length of the seismic activation stage and the magnitude.
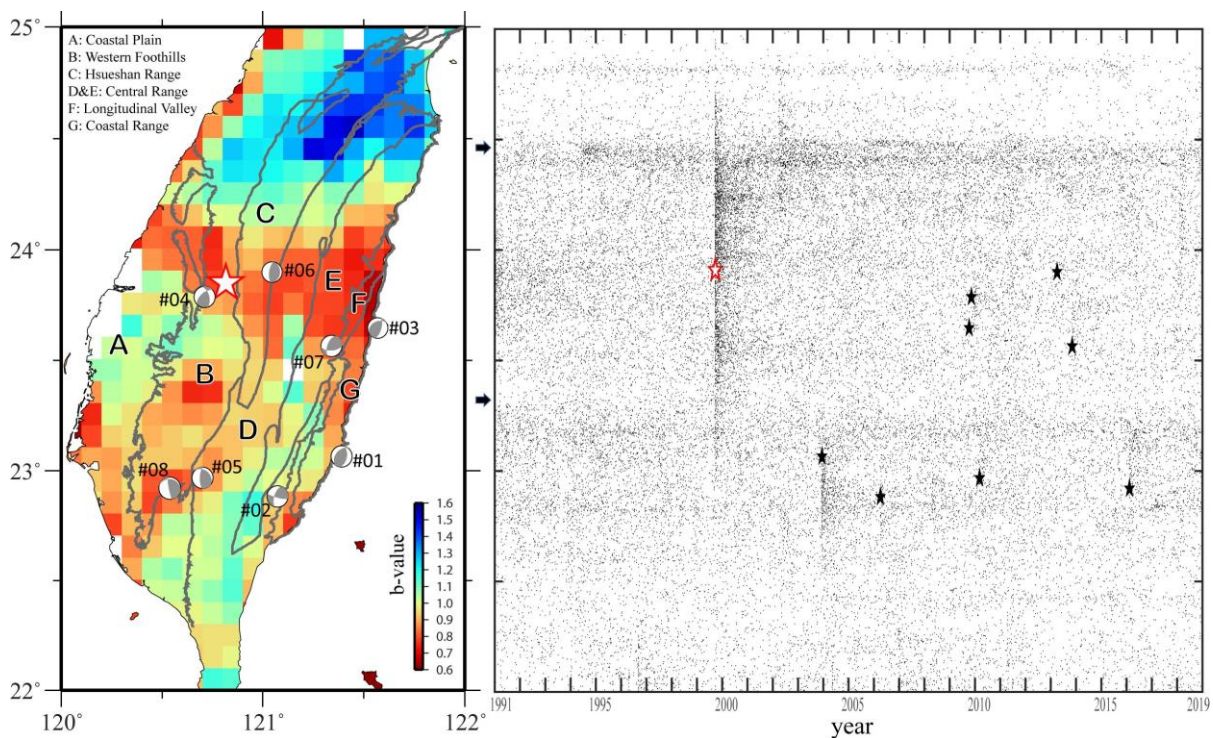
Figure 3: Map view of the earthquake b-value and declustered seismicity distribution as a function of time and latitude. The white star indicates the 1999 Chi-Chi earthquake, and the black stars (or focal mechanisms) represent the investigated events in this study. The black arrows indicate the seismicity boundaries. The major geological units in Taiwan are marked by gray curves and labeled from A to G.

149

3.2 Spatial Seismic Activation/Quiescence Distribution

Since Q-type and A-type events are located in southern and central Taiwan, respectively, it would be worth examining the spatial pattern of their abnormal seismicity stages. Wen and Chen (2017) pointed out that various seismic activation or quiescence processes of about 2–4 years were found prior to some events occurring in Taiwan (Chen and Wu, 2006; Wen et al., 2016; Wu et al., 2008). Thus, for consistency, we only consider the last abnormal stage within four years prior to the investigated events, as marked by red vertical lines for the quiescence stage of Q-type events and green vertical lines for the activation stage of A-type events. Then, we calculate the summation of the selected period to generate the seismic quiescence/activation distribution. Considering the definition of the weighted RTL function, a sufficient amount of background seismicity should be regarded as a criterion (Wen and Chen, 2017). Using the declustered catalog from 1991 to 2016, we set up two conditions similar to those of Wen and Chen (2017) for each grid to strengthen the reliability: (i) the total number of events within the grid area of $0.1°\times0.1°$ must be more than 26 (i.e., at least 1 event occurred every year on average); and (ii) the total events within a circle of $2r_0$ in radius must be more than 9360 (i.e., at least 30 events occurred every month on average). For each event, we normalize the spatial distribution based on the summed result. The spatial seismic activation/quiescence map provides the information of influence of surrounding seismicity state to the target event during the abnormal stage. Similar to previous studies (e.g., Huang et al., 2001; Huang and Ding, 2012), Fig. 4 shows that Q-type events mostly occurred on the edge of the seismic quiescence area; and seismic activation appeared around the A-type events.
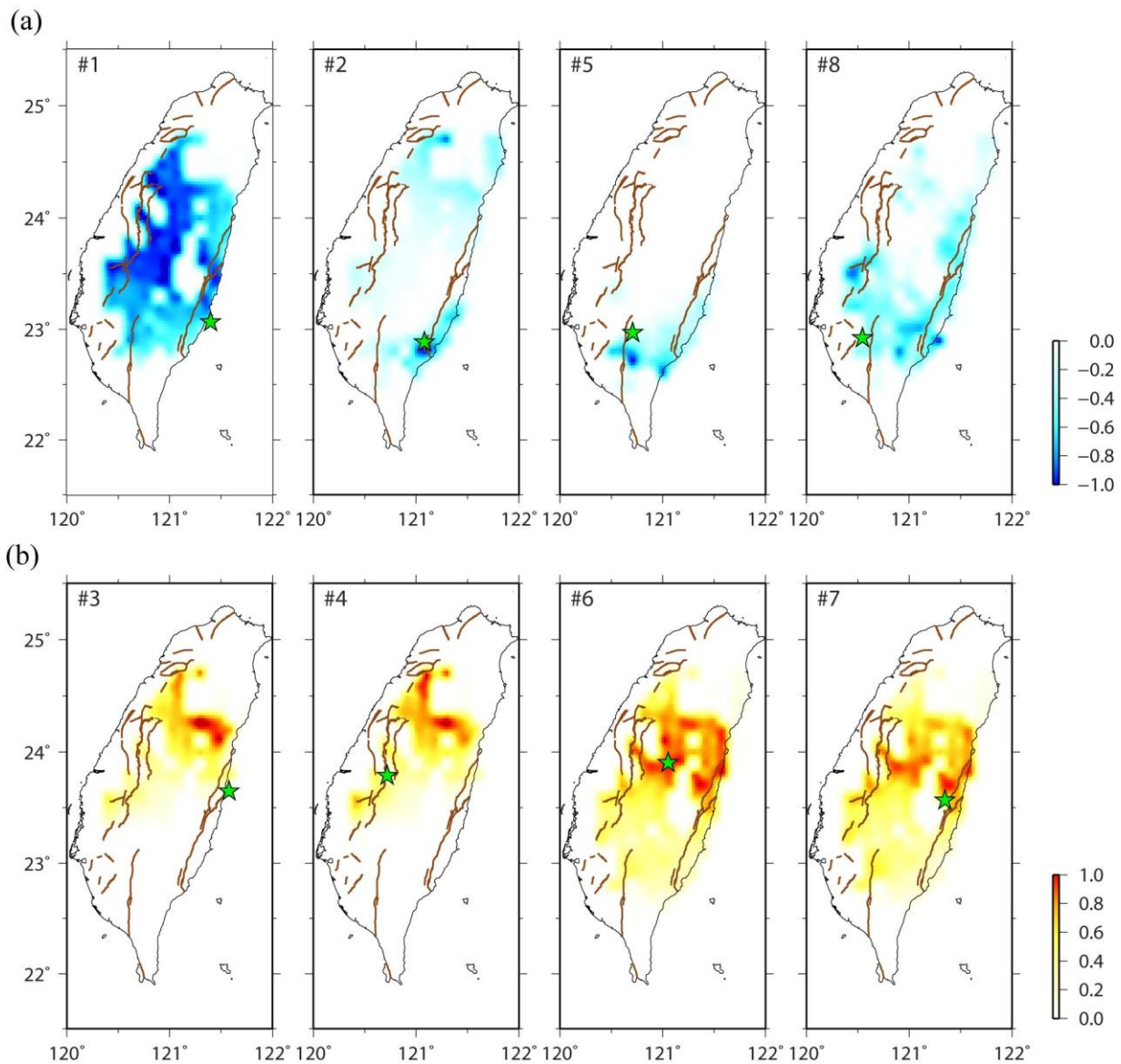
Figure 4: (a) The summed and normalized seismic quiescence map for the selected time window of the temporal RTL function of Q-type events, and (b) the summed and normalized seismic activation map for the selected time window of the temporal RTL function of A-type events. Stars represent the locations of the investigated events. The active faults (thick lines) identified by the Central Geological Survey of Taiwan are also shown.

173

174 **4. Discussion**

175 **4.1 Spatiotemporal Characteristics of Seismicity Changes**

176   The RTL analysis accounts for the background seismicity prior to the investigated

177 event. Therefore, the RTL analyses account for almost the same background period for

178 event Nos. 3 and 4 (1999-2009) and for event Nos. 6 and 7 (2003-2013), respectively.

179 As the temporal RTL functions show the seismic activation stage prior to the

180 mainshocks during a similar period, we could expect similar seismic activation maps for

181 event Nos. 3 versus 4 and event Nos. 6 versus 7, as shown in Fig. 4. Furthermore, the

182 seismic quiescence stage of event No. 5 occurred in a similar period as the seismic

183 activation stage of event No. 3 (Fig. 2), and the seismic quiescence area of event No. 5

184 complements the seismic activation area of event No. 3 (Fig. 4). In contrast, although

185 event Nos. 3 and 7 occurred at close locations, the difference in the 10-year background

186 period affects the weighting of the deviation. For example, the seismic quiescence stage

187 during 2007–2009 shown in the temporal RTL function of event No. 7 (Fig. 2) is

188 evaluated as the background seismicity level (RTL value is equal to zero) in the temporal

189 RTL function with respect to event No. 3. On the other hand, Wen and Chen (2017)

190 pointed out that an abnormal seismic stage derived with various background periods

191 cannot be produced by chance. The temporal RTL functions of five events (Nos. 1–5 in

192 Fig. 2) accounting for different background periods all exhibit the seismic quiescence

193 stage before the occurrence of event No. 1. This phenomenon is consistent with the

194 seismic quiescence map of event No. 1 (Fig. 4) and the Z-value map of Wu et al. (2008)

195 in which the seismic activity decreased during 2002–2003 for a large area in Taiwan. In

196 addition, the widespread seismic activation distribution of Nos. 6 and 7 (Fig. 4) also

197 responded to the seismic activity increase during 2011–2012 (Nos. 6–8 in Fig. 2). Wen

198 et al. (2016) suggested that, after the 2010 Jiashian earthquake (event No. 5), the 2-year

199 seismicity increase is caused by the increase in Coulomb stress change, which is

200 consistent with the seismic activation period in the temporal RTL function of event No.

201 8.

202 Rundle et al. (2000) proposed the self-organizing spinodal (SOS) model for

203 characteristic earthquakes and suggested that small earthquakes occurred uniformly at

204 all times, while the occurrence rate of intermediate-sized earthquakes varied during the

205 earthquake cycle. Chen (2003) investigated the SOS behavior of the 1999 Chi-Chi

206 earthquake and proposed the seismic activation of moderate-size (5<M<6) events prior

207 to the mainshock. Here, we also calculate the cumulative frequency–magnitude

208 distributions for these eight events using the same catalog periods of the RTL analysis.

209 For each investigated event, we only compared the distribution diagrams of the long-

210 term (background period) and abnormal seismic stages marked by dashed lines in Fig.

211 2, within a radius of 25 km with respect to the epicenter. As shown in Fig. 5, cumulative

212 frequency-magnitude distributions of long-term seismicity (red dots) generally exhibit

213 linear power law distributions. For the Q-type events, the cumulative frequency

214 distributions of the seismic quiescence stage (black dots) appear to lack 2.5<M<4.5

215 events (Fig. 5a), and the lack of a level corresponds to the seismic quiescence

216 distribution near the epicenter (Fig. 4). This indicates that within the seismic quiescence

217 stage before the occurrence of the Q-type event, the quiescence of 2.5<M<4.5 activity

218 contributes to the accumulation of tectonic stress.
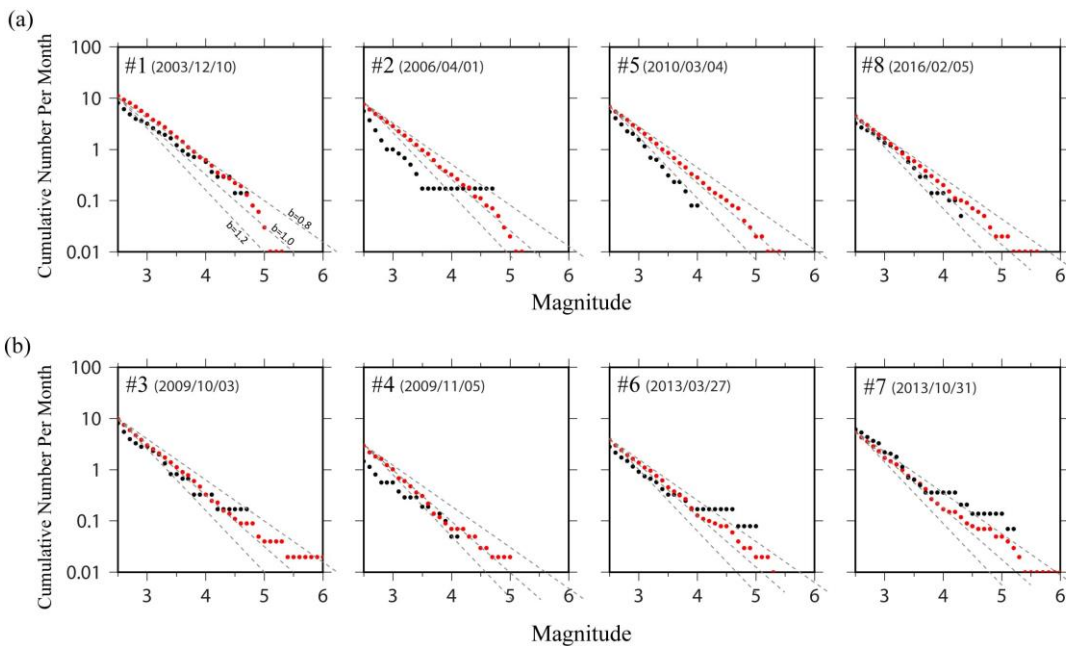
Figure 5: The cumulative frequency–magnitude distributions prior to the investigated events. Red and black dots represent the long-term and abnormal seismic stage marked in Fig. 2, respectively.

219

On the other hand, the cumulative frequency distributions of the seismic activation stage

of the A-type events (black dots in Fig. 5b) show that the seismic activation of 3<M<5

events within the seismic activation stage before the occurrence of the A-type

earthquake can be found, which is similar to the results of the 1999 Chi-Chi earthquake

(Chen, 2003). Event Nos. 6 and 7, which are located very close to the high seismic

activation area (Fig. 4), display the more obvious increase in the number of 4<M<5

events during the seismic activation stage (Fig. 5b).

Event No. 4 occurred only one month later than event No. 3; however, the seismic

activation stage of event No. 4 was much longer than that of event No. 3. Furthermore,

the cumulative frequency distributions of the seismic activation stage of event No. 4

display a lower intercept (Fig. 5b), which represents the overall decreasing seismicity

within this seismic activation stage. Here, we further divide the seismic activation stage

of event No. 4 into three periods for discussion: (i) P1: 2008/02–2009/03 before the

seismic activation stage of event No. 3; (ii) P2: 2009/04–2009/09 matching the seismic

activation stage of event No. 3; and (iii) P3: 2009/10 between the occurrences of event

Nos. 3 and 4. The seismic activation distributions in Fig. 6 are all normalized with

respect to the maximum RTL value of the seismic activation distribution of event No. 4

through Periods P1–P3. We can see that before the seismic activation stage of event No.

3 during 2008/02–2009/03 (P1), the location of event No. 3 indeed shows no seismic

activation, as exhibited in the temporal RTL function (Fig. 2b). On the other hand, for

the location of event No. 4, the seismic activation remains through all three Periods P1–

P3. Combined with the overall decreasing seismicity indicated by the lower intercept in

Fig. 5(b), these results suggest that this seismic activation prior to event No. 4 was

mainly contributed by the relatively accelerating activity of 3.5<M<4 events.
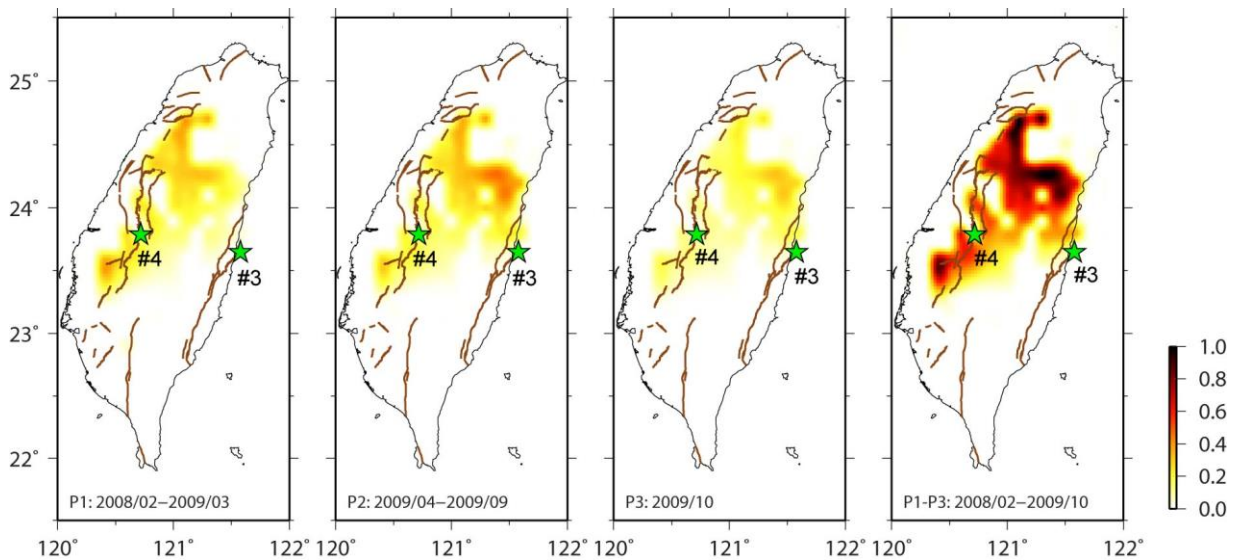
Figure 6: The summed seismic activation map for different periods of the seismic activation stage prior to event No. 4; all maps are normalized based on the summed results of P1–P3. Stars represent the locations of event Nos. 3 and 4. The active faults (thick lines) identified by the Central Geological Survey of Taiwan are also shown.

244

245   **4.2 Implication for the Tectonic Setting**

246   Several major active faults in southwestern Taiwan have been identified, and most

247   of them have been dominated by thrust movement. Some strike-slip structures, e.g., the

248   Zuochen and Hsinhua faults, acted as the transfer structures between these thrust faults

249   (Ching et al., 2011; Deffontaines et al., 1994, 1997; Rau et al., 2012). These transfer

250   structures develop at around 23°N, which is the northern limit of the Wadati–Benioff

251   zone (Kao et al., 2000) and close to the seismicity boundary indicated in Fig. 3. Geodetic

252   data displayed various rates and orientations of horizontal shortening with rapid uplift

253   rates in southern Taiwan (Fig. 1), which might be caused by underplating beneath the

254   Central Range sustaining crustal thickening and exhumation (Simoes et al., 2007). The

255   seismic b-value, which is the relative earthquake size distribution, can be derived from

256   the Gutenberg–Richter relation (Gutenberg and Richter, 1944): $\log N = a - bM$, where

257   constant *a* is related to seismicity and *N* is the number of earthquakes with magnitudes

258   greater than *M*. In general, a high b-value indicates a larger proportion of small events,

259   and a low b-value suggests that large earthquakes dominate over small ones. Using the

260   same declustered catalog from 1991 to 2018, we search for events within a radius of 25

261   km with respect to the center of each grid ($0.1° \times 0.1°$). Only for the grids with more than

262   30 events, we calculate the b-value using the weighted least-squares fitting method (Shi

263   and Bolt, 1982) and the spatial distribution of b-values, as shown in Fig. 3. The

264   seismicity in the southern Central Range is active but shows significant heterogeneity

265   in faulting types (Fig. 1; Chen et al., 2017; Wu et al., 2018), and relatively high b-values

266   suggest the predominance of small earthquakes in this region (Fig. 3 and red dots in Fig.

267   5a; Wu et al., 2018). Wen et al. (2016) found the decreased seismicity and increased

268   Coulomb stress change in the southern Central Range prior to the 2010 Jiashian

269   earthquake (i.e., event No. 5) and suggested both variations in Coulomb stress and

270   seismicity rate play important roles in contributing to the nucleation process of

271   impending earthquakes. The seismicity rate change can be considered a proxy for the

272   stress state change (Dieterich, 1994; Dieterich et al., 2000), and this implies that the

273   quiescence of seismicity contributes to the accumulation of tectonic stress. Since this

274   relatively high b-value region in the southern Central Range has been observed to have

275   a seismicity decrease (2.5<M<4.5 events) before the occurrence of Q-type events, it can

276   be an indicator of stress change.

277   Many devastating earthquakes with surface ruptures have occurred in the central

278   Taiwan, including the 1935 M 7.1 Hsinchu–Taichung earthquake, the 1951

279   Longitudinal Valley earthquake sequence and the 1999 Chi-Chi earthquake (Lee et al.,

280   2007; Chen et al., 2008; Lin et al., 2013). Hsu et al. (2009) derived the consistent

281   orientations of principal strain-rate and crust stress axes in central Taiwan, which

282   implies that faulting style corresponds to stress buildup accumulating from interseismic

283   loading (Fig. 1). They also pointed out that, for central Taiwan, small events tend to

284   surround the locked fault zone, where major earthquakes might occur, during the

285   interseismic period. The 1999 Chi-Chi earthquake ruptured the area near the end of the

286   décollement with a high contraction rate (Dominguez et al., 2003; Hsu et al., 2003;

287   2009). In addition, similar to the 1999 Chi-Chi earthquake, the A-type events occurred

288   in the low b-value area surrounded by small and active events. Chen and Wu (2006)

289   derived the temporal RTL function of the 1999 Chi-Chi earthquake, showing a pattern

290   similar to that of A-type events with the activation stage prior to the mainshock.

291   Furthermore, Wu (2006) calculated the seismic activation map of the 1999 Chi-Chi

292   event and found that the 1999 Chi-Chi mainshock occurred on the edge of the seismic

293   activation area, which is a low b-value region. This is similar to the seismic activation

294   maps of A-type events, which display the hot-spot pattern contracting within the low b-

295   value area (Figs. 3 and 4). The nucleation of the A-type mainshock can be attributed to

296   the perturbation of background seismicity (3<M<5 events) by the stress state change

297   (Dieterich, 1994; Dieterich et al., 2000).

298   The cumulative frequency distributions of long-term seismicity in Fig. 5 show a b-

299   value of 0.8–1.0 around these eight events, which is consistent with the pattern shown

300   in Fig. 3. However, the cumulative frequency distributions of long-term seismicity

301   exhibit different trends of magnitudes larger than 4.5 for the two types of events. The

302   seismicity for M>4.5 events is lower in the area around the Q-type event but higher in

303   the area around the A-type event. Event Nos. 1, 2, 3 and 7 occurred in eastern Taiwan

304   with an average GPS velocity of about 60 mm/yr (Fig. 1), and the cumulative frequency

305   distributions of long-term seismicity display a high intercept (Fig. 5). This rapid

306   convergence rate generally remains in the western part of southern Taiwan, which

307   indicates that only a little shortening is consumed from east to the west in southern

308   Taiwan. This corresponds to the active seismicity of small earthquakes, as indicated by

309 the high intercept of the cumulative frequency distributions of long-term seismicity for

310 event Nos. 1, 2, 5 and 8 (Fig. 5). Therefore, for the pre-collisional rapid and

311 distributed convergence in southern Taiwan (Shyu et al., 2005a), the quiescence of

312 $2.5<M<4.5$ activity contributes to the accumulation of tectonic stress for preparing for

313 the occurrence of the Q-type event. On the other hand, the shortening rate is obviously

314 consumed in the mountainous area of central Taiwan. Therefore, the lowest intercept of

315 the cumulative frequency distributions of long-term seismicity for event No. 4 (Fig. 5)

316 reflects the slow GPS velocity and low seismicity in the western part of central Taiwan

317 (Fig. 1). For central Taiwan, small events tend to surround the locked fault zone of the

318 potential major events during the interseismic period, and the 1999 Chi-Chi earthquake

319 is the case affected by the accelerating seismicity of moderate-size events and ruptured

320 the area near the end of the décollement with a high contraction rate (Chen, 2003;

321 Dominguez et al., 2003; Hsu et al., 2003; 2009). Tectonic stress accumulating from the

322 interseismic loading with the perturbation of the accelerating activity of $3<M<5$ events

323 could promote the nucleation process of the A-type event. The mechanisms causing

324 these different phenomena are not clear, and further study is still needed. For example,

325 some studies using machine-learning-based earthquake detectors and template-

326 matching techniques will be helpful to build a more complete earthquake catalog in

327 Taiwan (Liao et al., 2021; Zhai et al., 2021) and to get more useful data on small

328 earthquakes with a magnitude below 2.5.

329

330 **5. Conclusion**

331   Through statistical analyses of recent large earthquakes that occurred in Taiwan, we

332 summarize various temporal and spatial seismicity patterns prior to the earthquakes that

333 nucleated in different regions of Taiwan:

334   •   Q-type events occurred in southern Taiwan, with the northern boundary of

335   23.2°N, and experienced a seismic quiescence stage prior to the mainshock.

336   A seismicity decrease of 2.5<M<4.5 events in the relatively high b-value

337   southern Central Range could be an indicator of stress change related to the

338   preparation process of such events.

339   •   A-type events occurred in central Taiwan and experienced a seismic

340   activation stage prior to the mainshock, which nucleated on the edge of the

341   seismic activation area. We should consider when accelerating seismicity

342   of 3<M<5 events appears within the low b-value area.

343   Our results show that the spatiotemporal seismicity variations during the

344 preparation process of impending earthquakes could display a distinctive pattern

345 corresponding to the tectonic setting.

346
347

348   Appendix A

349   In the systematic correlation analysis for searching the optimal model parameters,

350   we calculate various combinations of r_0 (ranging between 25 and 80 km with a step of

351   2.5 km) and t_0 (ranging between 0.25 and 2.0 yr with a step of 0.05 yr). As the correlation

352   coefficient criterion C_0 is set, we can calculate the ratio W (or weight) of the combination

353   with correlation coefficients equal to or larger than C_0 for each model parameter of r_{0i}

354   ($i=1\sim m$; $m=23$) and t_{0j} ($j=1\sim n$; $n=36$). Then, the contour map for the ratio W is generated,

355   as shown in Fig. A1.

356
$$W_{ij} = \frac{\sum_{k=1}^{m} I(C_{ik} \geq C_0) + \sum_{l=1}^{n} I(C_{jl} \geq C_0)}{m+n} \tag{A1}$$

357   where the logical function $I(\Phi)$ is defined as

358
$$I(\Phi) = \begin{cases} 1, & \Phi \ is \ true \\ 0, & otherwise \end{cases} \tag{A2}$$

359   As the criterion ratio W_0 is set, the optimal model parameters, $\widetilde{r}_0$ and $\widetilde{t}_0$, can be

360   obtained by the following formulas:

361
$$\widetilde{r}_0 = \frac{\sum_{j=1}^{n} \sum_{i=1}^{m} W_{ij} I(W_{ij} \geq W_0) r_{0i}}{\sum_{j=1}^{n} \sum_{i=1}^{m} W_{ij} I(W_{ij} \geq W_0)} \tag{A3}$$

362
$$\widetilde{t}_0 = \frac{\sum_{i=1}^{m} \sum_{j=1}^{n} W_{ij} I(W_{ij} \geq W_0) t_{0j}}{\sum_{i=1}^{m} \sum_{j=1}^{n} W_{ij} I(W_{ij} \geq W_0)} \tag{A4}$$

363   Using event No. 6 as an example, we considered criterion coefficient $C_0 = 0.6$ and

364   criterion ratio $W_0 = 0.5$, which indicates that at least 50% of the total combination pairs

365   had a correlation coefficient $C \geq C_0 = 0.6$. Then, we obtained $\widetilde{r}_0 = 50.0$ km and $\widetilde{t}_0 = 1.14$

366   yr (diamond in Fig. A1) by averaging the parameter values that passed the criterion.

367   In addition, Nagao et al. (2011) proposed the RTM algorithm to reduce the dual

368   effect of the distance (r_i) by introducing the new factor

369
$$M(x,y,z,t) = \left[\sum_{i=1}^{n}(M_i)\right] - M_{bk}(x,y,z,t) \tag{A4}$$

370   where M_i is the earthquake magnitude of the ith prior event. Here, we also calculate the

371   RTM function of each investigated event with the same characteristic parameter set of

372   the RTL model, and both functions display very similar trends with minor differences,

373   as shown in Figure R2. The reason for this could be that, for these eight events, no large

374   earthquakes occurred in the vicinity of the epicenter. The bar chart in Fig. A2, which

375   represents the occurrence time of M ≥ 6.0 events within a distance of $2r_0$ from the target

376   event, also supports this explanation.
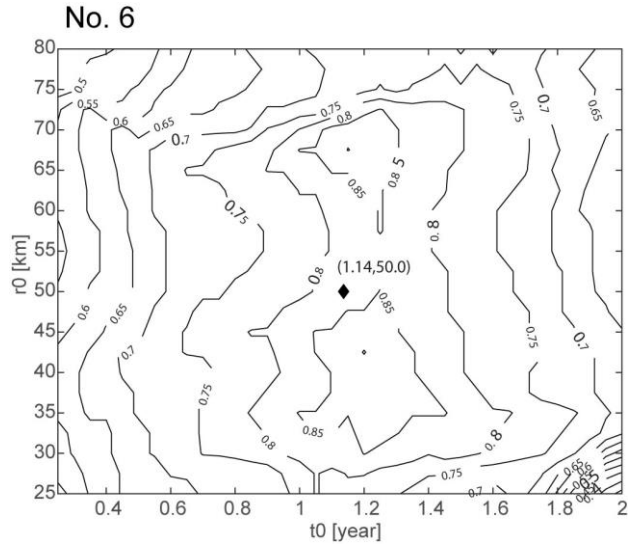
Figure A1: Contour map of ratio W for various combinations of model parameters of r_0 and t_0, with $C_0 = 0.6$ for event No. 6. The diamond shows the optimal model parameters as selecting criterion ratio $W_0 = 0.5$.

377
378
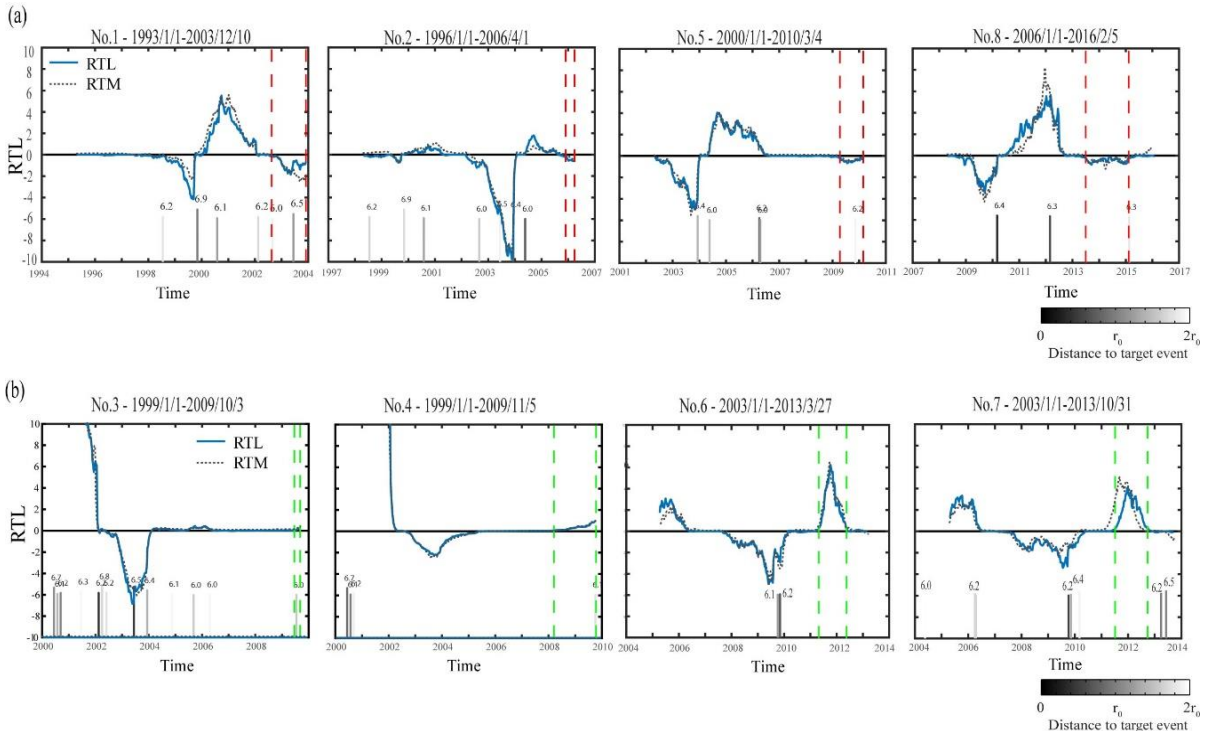
Figure A2: Temporal variation of the RTL (solid line) and RTM (dotted line) functions for (a) Q-type events and (b) A-type events. The bar chart represents the occurrence time of M ≥ 6.0 events within a distance of $2r_0$ from the target event; each number above the bar is the magnitude.

379   **Data Availability :** The seismic data is available in the Geophysical Database

380   Management System (GDMS, https://gdms.cwb.gov.tw/). A Chinese manual for data

381   access from the GDMS is on the website.

382

383   **Author contributions**: Conceptualisation, YYW, CCC; Investigation, YYW, WTL;

384   Validation, Formal analysis, Writing - original draft preparation, YYW; Writing -

385   review & editing, YYW, CCC, SW.

386

387   **Competing interests**: The authors declare no conflicts of interest.

388

389   **Acknowledgments:** We thank Central Weather Bureau (CWB) of Taiwan for providing

390   seismic data. This research was supported by the Ministry of Science and Technology

391   in Taiwan with grant: MOST 110-2116-M-194-018. The Taiwan Earthquake Center

392   (TEC) contribution number for this article is ****.

393

394

References:

Chan, C.H., Wu, Y.M., Tseng, T.L., Lin, T.L., and Chen, C.C.: Spatial and temporal evolution of b-values before large earthquakes in Taiwan. *Tectonophysics*, **532**, 215-222, 2012.

Chen, C.-C., Rundle, J.B., Holliday, J.R., Nanjo, K.Z., Turcitte, D.L., Li, S.C., and Tiampo, K. F.: The 1999 Chi-Chi, Taiwan, earthquake as a typical example of seismic activation and quiescence. *Geophys. Res. Lett*., **32**(22), L22315, doi:10.1029/2005GL023991, 2005.

Chen, C.C., and Wu, Y.X.: An improved region–time–length algorithm applied to the 1999 Chi-Chi, Taiwan earthquake. *Geophys. J. Int.*, **166**, 1144-1147, doi 10.1111/j.1365-246X.2006.02975.x, 2006.

Chen, J.S., Ching, K.E., Rau, R.J., Hu, J.C., Cheng, K.C., Chang, W.L., Chuang, R.Y., Chen, C.L., and Chen, H.C.: Surface deformation in Taiwan during 2002-2017 determined from GNSS and precise leveling measurements. Central Geological Survey Special Publication, 33, 157-178, 2018. (in Chinese with English abstract)

Chen, K.H., Toda, S., and Rau, R.J.: A leaping, triggered sequence along a segmented fault: the 1951 Hualien – Taitung earthquake sequence in eastern Taiwan. *J. Geophys. Res*., **113**, B02304, doi:10.1029/2007JB005048, 2008.

Chen, S.K., Wu, Y.M., Hsu, Y.J., and Chan, Y.C.: Current crustal deformation reassessed by cGPS strain-rate estimation and focal mechanism stress inversion. *Geophys. J. Int.*, **210**, 228–239. https://doi.org/10.1093/gji/ggx165, 2017.

Ching, K.E., Johnson, K.M., Rau, R.J., Chuang, R.Y., Kuo, L.C., and Leu, P.L.: Inferred fault geometry and slip distribution of the 2010 Jiashian, Taiwan, earthquake is consistent with a thick-skinned deformation model. *Earth Planet. Sci. Lett*., EPSL-S-10-00445, doi:10.1016/j.epsl.2010.10.021, 2011.

420   Deffontaines, B., Lee, J.-C., Angelier, J., Carvalho, J., and Rudant, J.-P.: New

421   geomorphic data on the active Taiwan orogen: a multisource approach. *J. Geophys.*

422   *Res.*, **99**, 20243–20266, 1994.

423   Deffontaines, B., Lacombe, O., Angelier, J., Mouthereau, F., Lee, C.T., Deramond, J.,

424   Lee, J.F., Yu, M.S., and Liu, P.M.: Quaternary transfer faulting in Taiwan Foothills:

425   evidence from a multisource approach. *Tectonophysics*, **274**, 61–82, 1997.

426   Dieterich, J. H.: A constitutive law for rate of earthquake production and its application

427   to earthquake clustering. *J. Geophys. Res*., **99** (18), 2601-2618, 1994.

428   Dieterich, J., Cayol, V., and Okubo, P.: The use of earthquake rate changes as a stress

429   meter at Kilauea volcano. *Nature*, **408**, 457–460, 2000.

430   Dominguez, S., Avouac, J.P., and Michel, R.: Horizontal coseismic deformation of the

431   1999 Chi-Chi earthquake measured from SPOT satellite images: implications for

432   the seismic cycle along the western foothills of central Taiwan. *J. Geophys. Res*.,

433   **108**, doi:10.1029/2001JB000951, 2003.

434   Gardner, J. K., and Knopoff, L.: Is the sequence of earthquakes in Southern California,

435   with aftershocks removed, Poissonian?. *Bull. Seis. Soc. Am*., **64**(5), 1363-1367,

436   1974.

437   Gutenberg, B., and Richter, C.F.: Frequency of earthquakes in California. *Bull. seism.*

438   *Soc. Am*., **34**, 185–188, 1944.

439   Hsu, Y.J., Kao, H., Bürgmann, R., Lee, Y.T., Huang, H.H., Hsu, Y.F., and Zhuang, J.:

440   Synchronized and asynchronous modulation of seismicity by hydrological loading:

441   A case study in Taiwan. *Sci. Adv.*, **7** (16), p. eabf7282, doi: 10.1126/sciadv.abf7282,

442   2021.

Hsu, Y.J., Simons, M., Yu, S.B., Kuo, L.C., and Chen, H.Y.: A two-dimensional dislocation model for interseismic deformation of the Taiwan mountain belt. *Earth Planet. Sci. Lett.*, **211**, 287–294, 2003.

Hsu, Y.J., Yu, S.B., Simons, M., Kuo, L.C., and Chen, H.Y.: Interseismic crustal deformation in the Taiwan plate boundary zone revealed by GPS observations, seismicity, and earthquake focal mechanisms. *Tectonophysics*, **479**, 4–18. https://doi.org/10.1016/j.tecto.2008.11.016, 2009.

Huang, Q., and Ding, X.: Spatiotemporal variations of seismic quiescence prior to the 2011 M 9.0 Tohoku earthquake revealed by an improved Region-Time-Length algorithm. *Bull. Seismol. Soc. Am.,* **102**(4), 1878-1883, doi: 10.1785/0120110343, 2012.

Huang, Q., Sobolev, G.A., and Nagao, T.: Characteristics of the seismic quiescence and activation patterns before the M=7.2 Kobe earthquake. *Tectonophysics,* **337**, 99-116, 2001.

Kao, H., Huang, G.C., and Liu, C.S.: Transition from oblique subduction to collision in the northern Luzon arc-Taiwan region: Constraints from bathymetry and seismic observations. *J. Geophys. Res*., **105**, 3059-3079, 2000.

Kasahara, K.: Earthquake Mechanics, *Cambridge Univ. Press., Cambridge*, 248 pp., 1981.

Lee, S.J., Chen, H.W., and Ma, K.F.: Strong Ground Motion Simulation of the 1999 Chi-Chi, Taiwan, Earthquake from a Realistic 3D Source and Crustal Structure. *J. Geophys. Res.*, **112**, B06307, doi: 10.1029/2006JB004615, 2007.

Liao, W. Y., Lee, E. J., Mu, D., Chen, P., and Rau, R. J.: ARRU phase picker: Attention recurrent-residual U-Net for picking seismic P-and S-phase arrivals. *Seismol. Res. Lett.*, **92**(4), 2410-2428, 2021.

468   Lin, D.-H., Chen, H., Rau, R.-J., and Hu, J.-C.: The role of a hidden fault in stress

469   triggering: Stress interactions within the 1935 Mw 7.1 Hsinchu–Taichung

470   earthquake sequence in central Taiwan. *Tectonophysics*, **601**, 37-52, doi:

471   10.1016/j.tecto.2013.04.022, 2013.

472   Lu, W. T.: Seismicity Changes Prior to the M>6 Earthquakes in Taiwan During 1993 to

473   2016 - an Approach of the RTL Algorithm. M.Sc. thesis, National Chung Cheng

474   University, Taiwan, p 66, 2017. (in Chinese with English abstract)

475   Mignan, A., and Giovambattista, R. Di: Relationship between accelerating seismicity

476   and quiescence, two precursors to large earthquakes. *Geophys. Res. Lett.*, **35**,

477   L15306, doi:10.1029/2008GL035024, 2008.

478   Rau, R.J., Lee, J.C., Ching, K.E., Lee, Y.H., Byrne, T.B., and Chen, R.Y.: Subduction-

479   continent collision in southwestern Taiwan and the 2010 Jiashian earthquake

480   sequence. *Tectonophysics*, **578**, 107-116, doi:10.1016/j.tecto.2011.09.013, 2012.

481   Rundle, J.B., Klein, W., Turcotte, D.L., and Malamud, B.D.: Precursory seismic

482   activation and critical point phenomena. *Pure Appl. Geophys.*, **157**, 2165-2182,

483   doi:10.1007/PL00001079, 2000.

484   Simoes, M., Avouac, J.P., Beyssac, O., Goffe, B., Farley, K.A., and Chen, Y.G.:

485   Mountain building in Taiwan: a thermokinematic model. *J. Geophys. Res.*, **112**.

486   doi:10.1029/2006JB004824, 2007.

487   Shi, Y., and Bolt, B.A.: The standard error of the magnitude-frequency b value. *Bull.*

488   *seism. Soc. Am.*, **72**, 1677–1687, 1982.

489   Shyu, J. B. H., Sieh, K., and Chen, Y.-G.: Tandem suturing and disarticulation of the

490   Taiwan orogen revealed by its neotectonic elements. *Earth Planet. Sci. Lett.*, **233**,

491   167–177, 2005a.

492 Shyu, J.B.H., Sieh, K., Chen, Y.-G., and Liu, C.-S.: Neotectonic architecture of Taiwan

493   and its implications for future large earthquakes. *J. Geophys. Res.*, **110**, p. B08402,

494   doi: 10.1029/2004JB003251, 2005b.

495 Sobolev, G.A., and Tyupkin, Y.S.: Low-seismicity precursors of large earthquakes in

496   Kamchatka. *Volc. Seismol.*, **18**, 433-446, 1997.

497 Sobolev, G.A., and Tyupkin, Y.S.: Precursory phases, seismicity precursors, and

498   earthquake prediction in Kamchatka. *Volc. Seismol.*, **20**, 615-627, 1999.

499 Suppe, J.: Kinematics of arc-continent collision, flipping of subduction, and backarc

500   spreading near Taiwan. *Mem. Geol. Soc. China*, 21–33, 1984.

501 Wang, J.H.:. The Taiwan Telemetered Seismographic Network. *Phys. Earth Planet.*

502   *Inter.*, **58**, 9–18, 1989

503 Wang, J.H., Chen, K.C., and Lee, T.Q.: Depth distribution of shallow earthquakes in

504   Taiwan. *J. Geol. Soc. China*, **37**, 125–142, 1994.

505 Wen, Y.-Y., Chen, C.-C., Wu, Y.-H., Chan, C.-H., Wang, Y.-J., and Yeh, Y.-L.:

506   Spatiotemporal investigation of seismicity and Coulomb stress variations prior to

507   the 2010 ML 6.4 Jiashian, Taiwan earthquake. *Geophys. Res. Lett.*, **43**,

508   doi:10.1002/2016GL070633, 2016.

509 Wen, Y.-Y., and Chen, C.-C.: Seismicity variations prior to the 2016 ML 6.6 Meinong,

510   Taiwan earthquake. *Terr. Atmos. Ocean. Sci.*,**28**, 737-742, doi:

511   10.3319/TAO.2016.12.05.01, 2017.

512 Wu, Y. H.: An improved region–time–length algorithm applied to the 1999 Chi-Chi,

513   Taiwan earthquake. M.Sc. thesis, National Central University, Taiwan, p 115, 2006.

514   (in Chinese with English abstract)

515 Wu, Y.M., and Chiao, L.Y.: Seismic Quiescence before the 1999 Chi-Chi, Taiwan, Mw

516   7.6 Earthquake. *Bull. Seismol. Soc. Am.*, **96**, 321-327, doi: 10.1785/0120050069,

517   2006.

518 Wu, Y.M., Chen, C.-C., Zhao, L., and Chang, C.-H.: Seismicity characteristics before

519   the 2003 Chengkung, Taiwan, earthquake. *Tectonophysics*, **457**, 177-182, doi:

520   10.1016/j.tecto.2008.06.007.

521 Wu, Y.M., Chen, S. K., Huang, T.C., Huang, H.-H., Chao, W.A., and Koulakov, I.:

522   Relationship between earthquake b-values and crustal stresses in a young orogenic

523   belt. *Geophys. Res. Lett.*, **45**, 1832-1837, doi:10.1002/2017GL076694, 2018.

524 Wu, Y.M., Hsu, Y.J., Chang, C.H., Teng, L.S., and Nakamura, M.: Temporal and spatial

525   variation of stress field in Taiwan from 1991 to 2007: Insights from comprehensive

526   first motion focal mechanism catalog. *Earth Planet. Sci. Lett.*, **298**, 306–316.

527   https://doi.org/10.1016/j.epsl.2010.07.047, 2010.

528 Wyss, M., and Stefansson, R.: Nucleation points of recent mainshocks in Southern

529   Iceland, mapped by b-values. *Bull. Seismol. Soc. Am.*, **96**, 599–608, 2006.

530 Yu, S.B., Chen, H.Y., and Kuo, L.C.: Velocity field of GPS stations in the Taiwan area.

531   *Tectonophysics*, **274**(1-3), 41–59. https://doi.org/10.1016/S0040-1951(96)00297-1,

532   1997.

533 Zhai, Q. S., Peng, Z. G., Chuang, L. Y., Wu, Y. M., Hsu, Y. J., and Wdowinski, S.:

534   Investigating the Impacts of a Wet Typhoon on Microseismicity: A Case Study of

535   the 2009 Typhoon Morakot in Taiwan Based on a Template Matching Catalog. *J.*

536   *Geophys. Res.*, **126**(12). https://doi.org/10.1029/2021JB023026, 2021.

537